B-Side Charge Separation in Bacterial Photosynthetic Reaction Centers: Nanosecond Time Scale Electron Transfer from H_B^- to Q_B[†]

Christine Kirmaier,[‡] Philip D. Laible,[§] Deborah K. Hanson,[§] and Dewey Holten*,[‡]

Department of Chemistry, Washington University, St. Louis, Missouri 63130, and Biosciences Division, Argonne National Laboratory, Argonne, Illinois 60439

Received October 8, 2002; Revised Manuscript Received December 6, 2002

ABSTRACT: We report time-resolved optical measurements of the primary electron transfer reactions in *Rhodobacter capsulatus* reaction centers (RCs) having four mutations: Phe(L181) → Tyr, Tyr(M208) → Phe, Leu(M212) → His, and Trp(M250) → Val (denoted YFHV). Following direct excitation of the bacteriochlorophyll dimer (P) to its lowest excited singlet state P*, electron transfer to the B-side bacteriopheophytin (H_B) gives $P^+H_B^-$ in ∼30% yield. When the secondary quinone (Q_B) site is fully occupied, $P^+H_B^-$ decays with a time constant estimated to be in the range of 1.5−3 ns. In the presence of excess terbutryn, a competitive inhibitor of Q_B binding, the observed lifetime of $P^+H_B^-$ is noticeably longer and is estimated to be in the range of 4−8 ns. On the basis of these values, the rate constant for $P^+H_B^- \rightarrow P^+Q_B^-$ electron transfer is calculated to be between $\sim(2\text{ ns})^{-1}$ and $\sim(12\text{ ns})^{-1}$, making it at least an order of magnitude smaller than the rate constant of $\sim(200\text{ ps})^{-1}$ for electron transfer between the corresponding A-side cofactors ($P^+H_A^- \rightarrow P^+Q_A^-$). Structural and energetic factors associated with electron transfer to Q_B compared to Q_A are discussed. Comparison of the $P^+H_B^-$ lifetimes in the presence and absence of terbutryn indicates that the ultimate (i.e., quantum) yield of $P^+Q_B^-$ formation relative to P* is 10−25% in the YFHV RC.

The bacterial reaction center (RC)[1] is a membrane-bound pigment−protein complex within which a series of electron transfer reactions takes place on the sub-nanosecond time scale to convert light energy into chemical potential energy. The pigment cofactors are arranged with macroscopic C_2 symmetry and consist of four bacteriochlorophyll molecules (B), two of which form the dimeric primary electron donor (P), two bacteriopheophytins (H), and two quinones (Q) (Figure 1). These cofactors are embedded in polypeptide subunits L and M, also arranged in a nearly C_2 symmetric fashion, and give rise to the so-called A side and B side (or branches) of the RC (*1*−*5*). Upon absorption of light, P* transfers an electron within ∼4 ps to H_A utilizing B_A in parallel mechanisms as a discrete and virtual intermediate. The H_A anion subsequently transfers an electron in ∼200 ps to Q_A, leading to $P^+Q_A^-$ formation with an overall quantum yield of ∼1.

A working model for the wild-type RC in which $P^+B_A^-$ is below P* in free energy and $P^+B_B^-$ is above P* is shown in Figure 2A (*6*−*13*). Such a difference in the free energies of the P^+B^- states, coupled with possible differences in the electronic matrix elements for charge separation to the two sides (*12*−*21*), is thought to govern unidirectional electron transfer to the A-side cofactors. Recent work has shown that electron transfer to the B side can be elicited by several means, including increasing the free energy of $P^+B_A^-$ and/or reducing the free energy of $P^+B_B^-$ (*12*, *13*, *22*−*34*). Figure 2B gives a schematic free energy level diagram for some mutant RCs in which electron transfer to H_B has been observed. There is an ∼15% yield of $P^+H_B^-$ formation in the *Rhodobacter* (*Rb.*) *capsulatus* DH mutant G(M201)D/L(M212)H, where an Asp is placed near B_A at residue M201 (replacing a Gly) and a His is placed near H_A (*22*). A His at M212 causes H_A to be replaced with a bacteriochlorophyll molecule denoted β (*35*−*37*). Electron transfer to the B side

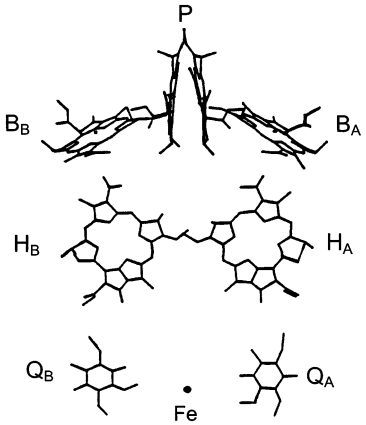

FIGURE 1: Arrangement of the RC cofactors, as determined by X-ray structures of RCs from *Rhodopseudomonas viridis* and *Rb. sphaeroides* (1−5).

[†] This work was supported by Grant MCB-0077187 from the National Science Foundation (D.H. and C.K.) and the U.S. Department of Energy, Office of Biological and Environmental Research, under Contract W-31-109-ENG-38 (P.D.L. and D.K.H.).

[‡] Washington University.

[§] Argonne National Laboratory.

[1] Abbreviations: P, bacteriochlorophyll dimer; B_A and B_B, monomeric bacteriochlorophylls; H_A and H_B, bacteriopheophytins; β, bacteriochlorophyll incorporated for bacteriopheophytin at the H_A site; Q_A and Q_B, primary and secondary quinone acceptors, respectively; RC, reaction center.

10.1021/bi026973o CCC: $25.00
Published on Web 01/28/2003

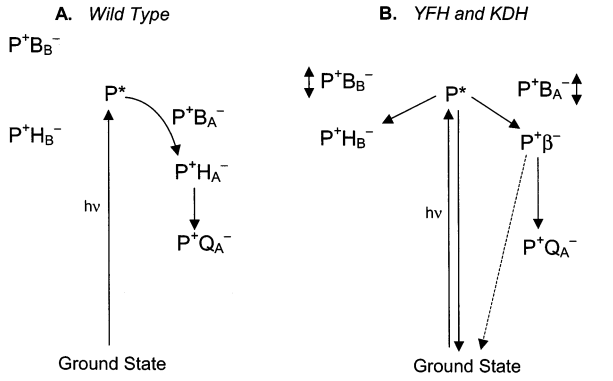

FIGURE 2: Schematic energy level diagrams for (A) the wild type and (B) the YFH and KDH mutant RCs. In the mutants, $P^+B_A^-$ is higher in free energy than in the wild type, and $P^+B_B^-$ lower. The double-headed arrows reflect uncertainty about whether these states are slightly above or slightly below P*.

in the DH mutant is suggested to result from a 100−150 meV destabilization of $P^+B_A^-$ caused by the presence of Asp-(M201) (*22*, *24*, *25*). Upon further introduction of a Lys residue near B_B (replacing a Ser at L178 to give the KDH mutant), the yield of $P^+H_B^-$ is increased to ∼23% (*23*). This increase is ascribed to the added effect of reducing the free energy of $P^+B_B^-$. Similar manipulation of the free energies of these states is accomplished in the YFH mutant (*12*), where the native Tyr residue at M208 is replaced with a Phe and the native Phe residue at L181 is replaced with a Tyr (again along with the Leu → His replacement at M212). Calculations and experiments had previously shown independently that the residues at M208 and L181 have an effect on the respective free energies of $P^+B_A^-$ and $P^+B_B^-$, and specifically that a nearby Tyr would have a strongly stabilizing effect (*6*, *7*, *32*, *38*−*50*). An ∼30% yield of electron transfer to H_B is found in the YFH mutant (*12*).

In recent work, we advanced these studies the next logical step and showed that the RC will support electron transfer further along the B-side pathway to cofactor Q_B. This result was initially observed in nanosecond-flash experiments on the *Rb. capsulatus* DHV mutant (*51*); the additional "V" mutation changes the native Trp residue at M250 to a Val, which inhibits binding of Q_A (*52*−*55*). In similar nanosecond-flash experiments on the *Rb. sphaeroides* DHW mutant (where the D and H mutations are equivalent to the ones described above and a W at M260 is used to inhibit binding of Q_A), a very small amount (≤3%) of $P^+Q_B^-$ formation was reported (*34*). Since Q_B is lost during the normal course of RC purification, it was reconstituted in both of these studies by addition of an excess of ubiquinone, with the M250 or M260 mutation preventing simultaneous reconstitution of the Q_A site. A premise of both these studies is that, with Q_A absent, formation of $P^+Q_B^-$ derives solely from $P^+H_B^- \rightarrow P^+Q_B^-$ electron transfer (i.e., from some amount of initial charge separation to the B side) since the normal $P^+Q_A^- \rightarrow P^+Q_B^-$ pathway is unavailable.

With an ∼30% yield of $P^+H_B^-$, the *Rb. capsulatus* YFH mutant RC affords the best opportunity to date to explore further details of B-side electron transfer to Q_B. To this end, we recently investigated YFHV RCs (V at M250) isolated with Q_B fully occupied from a strain of *Rb. capsulatus* that lacks LHI (*56*). With LHI absent, RCs that have full Q_B occupancy can be obtained by use of the mild detergent Deriphat 160-C for protein solubilization and purification. In YFHV RCs, we reported a >6 s time constant probing (at 860 nm) the decay of bleaching of the long wavelength absorption band of P. This time constant is assigned to $P^+Q_B^- \rightarrow$ ground state charge recombination (*56*). $P^+Q_B^-$ is distinguished from the $P^+Q_A^-$ state by a much longer lifetime for the former, on the order of seconds or tens of seconds depending on conditions, as opposed to a lifetime of ∼100 ms for $P^+Q_A^-$ (reviewed in refs *57* and *58*). Upon addition of excess terbutryn (a competitive inhibitor of Q_B binding) to YFHV RCs, the >6 s component is completely suppressed. Notably absent, also, are kinetics occurring on the millisecond time scale, confirming that Q_A is absent, as expected. The yield of $P^+H_B^- \rightarrow P^+Q_B^-$ electron transfer was estimated to be quite high in these experiments, possibly approaching 80%. However, multiple recycling of the RC photochemistry during the relatively long ∼7 ns excitation flashes will contribute to an accumulation of a population of RCs in the $P^+Q_B^-$ state that is larger than the population that actually results from a single turnover of the RC.

To directly measure the rate and yield of $P^+H_B^- \rightarrow P^+Q_B^-$ electron transfer, we have carried out an extensive series of ultrafast transient absorption experiments on YFHV RCs in the presence and absence of terbutryn. As noted above, using the detergent Deriphat 160-C to solubilize the RC directly yields samples with full occupancy of the Q_B site (*56*). With this critical element in place, ultrafast transient absorption measurements that probe for electron transfer to Q_B are readily possible without the intractable complication of partial and unquantifiable Q_B reconstitution in RC samples at the relatively high concentration needed for these experiments (∼35 μM). Use of the detergent Deriphat 160-C appears to result in some differences in the rates or yields of some of the primary electron transfer reactions (but not the $P^+H_B^-$ yield). These differences and a more complete description of the primary events in YFHV, YFH, and wild-type RCs in Deriphat and as compared to the same RCs in the detergent lauryldimethylamine *N*-oxide (LDAO) will be described in detail elsewhere (*59*). Here we focus specifically on $P^+H_B^- \rightarrow P^+Q_B^-$ electron transfer, with a goal of, first, demonstrating evidence for this process from changes in the transient absorption decay kinetics of $P^+H_B^-$ and, second, determining the rate and yield of this reaction. The results are discussed in comparison to the known ∼200 ps time constant and ∼100% yield for $P^+H_A^- \rightarrow P^+Q_A^-$ electron transfer on the A side of the RC.

EXPERIMENTAL PROCEDURES

Initial construction of the *Rb. capsulatus* YFH mutant and subsequent addition of the Val mutation at M250 to give polyhistidine-tagged YFHV RCs have been described previously (*12*, *56*). All of the samples studied here, YFHV, YFH, and the wild type, were prepared using the detergent Deriphat 160-C to solubilize the protein from strains of *Rb. capsulatus* that lack LHI. Experiments were conducted on RCs in a buffered solution consisting of 10 mM Tris (pH 7.6), 0.05% Deriphat 160-C, and 100 mM NaCl. A small aliquot of each sample was used in the nanosecond-flash experiments we reported previously that demonstrated that $P^+Q_B^-$ forms in the YFHV and YFH mutant RCs (*56*). The larger remaining portion of each preparation was used in the experiments we report here. On the basis of the various control measurements

described in detail previously (*56*), the samples we report on here are known to have full occupancy of the Q_B site and, in the case of YFHV RCs, full depletion of Q_A. The RC samples used here had an absorption at 865 nm that ranged from 0.9 to 1.05 (2 mm path length) corresponding to ~35 μM RCs. To obtain YFHV RCs devoid of Q_B, terbutryn was added from a 40 mM stock solution in ethanol to a final concentration of ~1 mM. The YFHV sample with no additions (fully Q_B occupied) will be called throughout simply YFHV. The YFHV sample with terbutryn added will be called YFHV+tb.

The time-resolved transient absorption instrument is based on an argon ion-pumped regeneratively amplified Ti:sapphire laser and optical parametric amplification system operated at 10 Hz. The RCs were excited with ~130 fs pulses at 860 nm and probed with ~130 fs "white-light" flashes. The excitation pulses were defocused and/or attenuated so that <30% of the RCs were excited on a single flash. A 2.5 mL sample of RCs, held in a reservoir cooled in an ice bath, was flowed through a 2 mm path length cell at sufficient speed that fresh RCs were delivered into the excitation region between the 10 Hz laser flashes. Compared to the 2.5 mL volume, only a fraction of a percent of the sample generates $P^+Q_B^-$ on a single flash. Dilution into the 2.5 mL volume of a flowed sample ensured that these RCs did not result in a "before-zero" signal in the ultrafast experiments despite the 6−10 s lifetime of $P^+Q_B^-$. A dual-diode array-based detection system provides transient absorption data encompassing an ~220 nm spectral window on a single flash. Further details of the apparatus, data acquisition, and data analysis methods have been described elsewhere (*60*, *61*).

RESULTS AND DISCUSSION

Yield of Electron Transfer to H_B. The yield of $P^* \rightarrow P^+H_B^-$ in the YFH mutant was previously determined to be ~30% in RCs purified with LDAO (12). The data shown in Figure 3 indicate that a similar yield is obtained in Deriphat-purified YFH and YFHV RCs. As was done previously, we determined the yield of $P^+H_B^-$ formation by comparing the magnitude of H_B bleaching at 527 nm with the magnitude of H_A bleaching at 542 nm for the $P^+H_A^-$ state in wild-type RCs. This process begins with comparison of the P* spectra shown in Figure 3A. Because the sample concentrations used in these experiments were closely matched (see Experimental Procedures) and because the laser excitation conditions vary only slightly from day to day, the raw amplitudes of the P* spectra acquired on the four samples were within 10% of one another. Three of the spectra shown in Figure 3A have been multiplied, by factors that ranged from 0.9 to 1.0, to normalize the magnitudes of initial P bleaching at 600 nm. The YFHV+tb sample was arbitrarily chosen as the base for the normalization, and its spectrum is the "raw" unnormalized data. The gently sloping absorption broken by bleaching of the Q_X band of P near 600 nm is characteristic of the difference spectrum of P* in this spectral window, and the P* spectra of all four samples are identical except for a slightly broader bleaching for the wild type.

The individual normalization factors for the YFHV, YFH, and wild-type RC samples used to generate the comparison in Figure 3A were applied to spectra taken at longer times

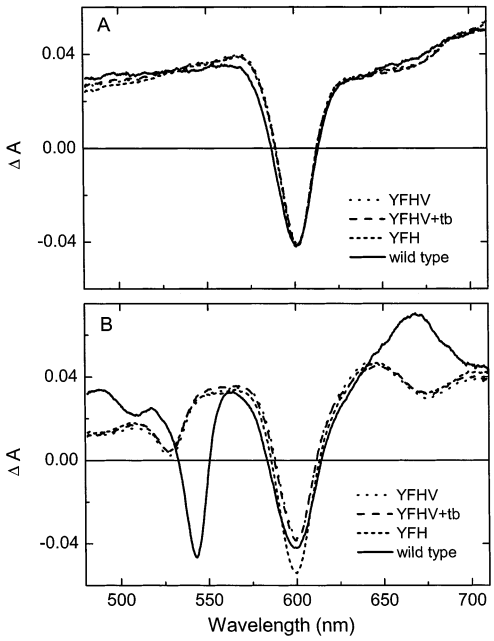

FIGURE 3: Comparison of the Q_X and anion region transient absorption difference spectra of YFHV, YFHV+tb, YFH, and wild-type RCs. Panel A shows the (normalized) P* spectra acquired 0.5 ps following excitation with ~130 fs flashes at 860 nm. Panel B shows spectra taken at ~100 ps (each of the three mutants) and at ~20 ps (wild type), multiplied by the same individual factors that were used in panel A. See the text for further details.

to yield the data shown in Figure 3B. For each sample, the spectrum that is shown was taken at a delay time that reflects the maximal bleaching of the H_A (wild type) or H_B (mutants) Q_X band. The absorption difference spectra for YFHV, YFHV+tb, and YFH RCs in Figure 3B are identical, except for a slightly larger bleaching near 600 nm in the YFH mutant. All three exhibit a pronounced bleaching of the Q_X band of H_B at ~527 nm. Because of the replacement of H_A with a bacteriochlorophyll molecule, β, the H_B bleaching in the mutants is not compromised (by spectral overlap) and can be compared directly with the bleaching at ~542 nm observed in the wild-type sample to obtain a yield of $P^+H_B^-$. The assumption underlying this comparison is that the Q_X bands of H_A and H_B have the same oscillator strength. On the basis of the data shown in Figure 3B, we calculate a 30−35% yield of $P^+H_B^-$ in the YFHV, YFHV+tb, and YFH samples. This is the same value within experimental error as reported previously for theYFH mutant in LDAO. Note also that neither the added V mutation nor the addition of terbutryn in the YFHV+tb sample gives rise to any differences in the shape or magnitudes of the spectra in Figure 3.

The prominent peak near 665 nm in the wild-type RC spectrum (Figure 3B) is the well-known absorption band of the anion of H_A. The peak of the analogous anion absorption band of H_B in the difference spectrum is near 640−650 nm. The H_B anion band is less pronounced in the difference spectra of the three mutant RCs, in keeping with the relatively low yield of $P^+H_B^-$ (~30%) compared to the 100% yield of $P^+H_A^-$ in wild-type RCs. Additionally relevant is the fact that whereas the 20 ps spectrum for wild-type RCs can be assigned to a single state, $P^+H_A^-$, this is not true for the ~100 ps spectra of the mutants. In these cases, the difference spectra reflect a composite of the absorption changes

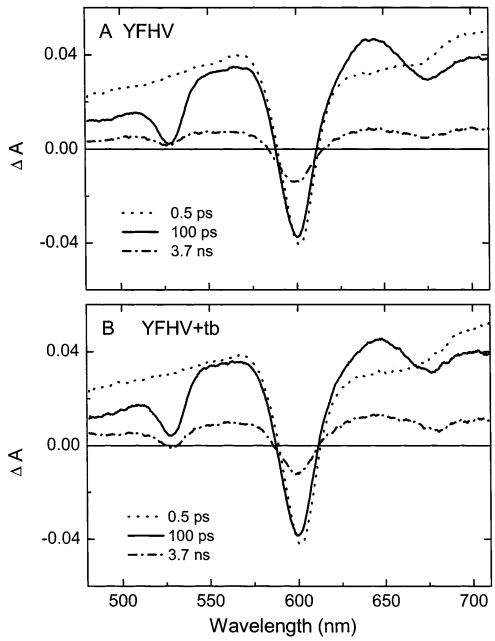

FIGURE 4: Transient absorption difference spectra for (A) YFHV and (B) YFHV+tb acquired at the indicated times following excitation with ~130 fs flashes at 860 nm.

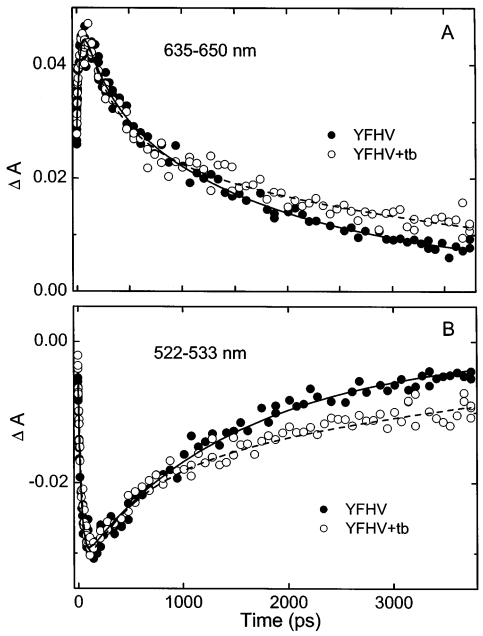

FIGURE 5: Comparison of kinetic data for YFHV and YFHV+tb, using ~130 fs excitation flashes at 860 nm. Data acquired before the flash and during the ~0.5 ps instrument rise time have been omitted for clarity. Panel A compares the kinetics of the transient absorption changes between 635 and 650 nm. Panel B plots the kinetic data for the appearance and decay of H_B bleaching between 522 and 533 nm minus the absorption changes between 570 and 585 nm (i.e., $\Delta A_{522-533} - \Delta A_{570-585}$). The solid (YFHV) and dashed (YFHV+tb) lines are fits to the sum of four exponentials along with a constant. See the text for further details.

resulting from electron transfer to H_B as well as to the β pigment on the A side [or any other state(s) that may have formed initially from P*].

Observation of $P^+H_B^- \rightarrow P^+Q_B^-$ Electron Transfer from Ultrafast Transient Absorption Data. Figure 4 replots the spectra shown in Figure 3 for YFHV (panel A) and YFHV+tb (panel B) RCs and compares them to spectra taken at 3.7 ns, the longest delay time available on our transient absorption instrument. At first glance, the 3.7 ns spectra of YFHV and YFHV+tb RCs are not noticeably dissimilar. However, the overall magnitudes of the absorption changes for YFHV+tb RCs are in fact slightly larger than those observed for YFHV RCs. The difference between the data on the nanosecond time scale is seen more readily in the kinetic profiles shown in Figure 5, which plots the time course of the absorbance changes in the range of 635−650 nm (the H_B anion absorption maximum) and in the range of 522−533 nm (the H_B Q_X band bleaching). For clarity of display, the points acquired before "zero time" and during the ~0.5 ps instrument rise time are not shown in Figure 5. Two slightly different sets of "matched" measurements were carried out to verify the fidelity of these results. For one set (that shown in Figure 5), a 5 mL sample of YFHV RCs was divided into two equal portions. Kinetic data were acquired on the first portion; then on the following day, terbutryn was added to the fresh unused second portion of the YFHV sample, and kinetic data for it were acquired. In the other set of measurements, one (fresh and unused) 2.5 mL sample of YFHV RCs was examined on a single day first without, and then with, terbutryn added. Somewhat fewer data points were acquired in this second set of measurements; however, the data reproduced the difference between YFHV and YFHV+tb samples shown in Figure 5.

The small difference between the YFHV and YFHV+tb kinetic profiles distinguishes the lifetimes of $P^+H_B^-$ in the presence and absence of Q_B and constitutes the first direct observation on the pico- to nanosecond time scale of $P^+H_B^-$ $\rightarrow$ $P^+Q_B^-$ electron transfer. These results complement the observation of $P^+Q_B^-$ formation from B-branch electron transfer in nanosecond-flash measurements on these YFHV RCs (*56*) and similar mutants (*34*, *51*). In principle, the data in Figure 5 straightforwardly determine the rate and yield of $P^+H_B^- \rightarrow P^+Q_B^-$ electron transfer. In the YFHV+tb sample (which lacks Q_B), the $P^+H_B^-$ lifetime (denoted τ_{TB}) reflects charge recombination of this state to the ground state because this is the only decay path available (and of course may involve $P^+B_B^-$ or P*). Thus, we can set τ_{TB} equal to $1/k_{CR}$, where k_{CR} is the rate constant for charge recombination (Scheme 1). In YFHV RCs, the $P^+H_B^-$ lifetime (denoted τ_{QB}) is equal to the inverse of the sum of k_{CR} and k_{ET}; i.e., $\tau_{QB} = 1/(k_{ET} + k_{CR})$, where k_{ET} is the rate constant of the $P^+H_B^- \rightarrow P^+Q_B^-$ electron transfer reaction. Thus, upon measurement of τ_{TB} and τ_{QB}, k_{ET} is determined as well as the yield of the $P^+H_B^- \rightarrow P^+Q_B^-$ reaction, given by $\Phi_{ET} = k_{ET}/(k_{ET} + k_{CR})$.

Scheme 1

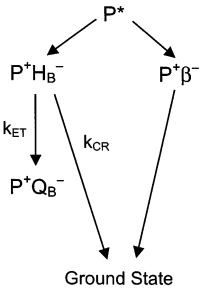

It is clear from visual inspection of the kinetic profiles in Figure 5 that the YHFV+tb data set the intrinsic (charge recombination) decay of $P^+H_B^-$ to be on the nanosecond time

scale, and that without terbutryn $P^+H_B^-$ still decays on the nanosecond time scale, somewhat faster but not dramatically so. These observations immediately lead to the qualitative conclusion that the rate constants for $P^+H_B^- \rightarrow P^+Q_B^-$ electron transfer (k_{ET}) and $P^+H_B^- \rightarrow$ ground state charge recombination (k_{CR}) are on the same order of magnitude, with values of several inverse nanoseconds or so. In the following section, we describe our detailed analysis of the kinetic data in Figure 5 that leads to ranges of $\sim(2-12\ \text{ns})^{-1}$ and $\sim(1.5-3\ \text{ns})^{-1}$ for k_{ET} and k_{CR}, respectively.

Estimates of the Rate and Yield of $P^+H_B^- \rightarrow P^+Q_B^-$ Electron Transfer. Let us consider qualitatively the anion region (635−650 nm) and the most simple kinetic model first. Such a model is based on the photochemistry shown in Scheme 1 and described above; P* decays to give both $P^+H_B^-$ and $P^+\beta^-$ which then decay independently on their respective B and A branches. $P^+\beta^-$ decays only via charge recombination to the ground state (because Q_A is absent due to the V mutation). $P^+H_B^-$ decays only via charge recombination to the ground state (with a rate constant k_{CR}) *or* via combined charge recombination and electron transfer to Q_B ($k_{ET} + k_{CR}$), depending on the absence or presence of Q_B, respectively. Thus, the most simple analysis is to fit the kinetic profiles to a function consisting of a constant long-time asymptote plus the sum of three exponentials: one for P* decay and one each for parallel independent decays of $P^+H_B^-$ and $P^+\beta^-$. Clearly, the only difference between the YFHV and YFHV+tb kinetic data, and the goal of this analysis, is the $P^+H_B^-$ lifetime.

The 635−650 nm kinetic profiles for both YFHV+tb and YFHV RCs display an initial fast phase of absorption increase that rises to a ΔA value of ∼0.05 on the 0.5−100 ps time scale. (This is again after the initial overall ∼0.5 ps instrument rise time, which is not shown in Figure 5.) This initial fast kinetic phase corresponds to the transformation of the 0.5 ps P* spectrum to the composite spectrum observed at ∼100 ps in Figure 4. Since electron transfer from P* occurs to both β on the A branch and H_B on the B branch, subsequent decay of the positive absorption at 635−650 nm (refer to the 100 ps spectra in Figure 4) must reflect contributions of the independent lifetimes of $P^+H_B^-$ and $P^+\beta^-$. The decay kinetics must reflect both lifetimes because (as alluded to above) the anions of both H_B and β absorb at 635−650 nm, although the former is expected to have the larger extinction coefficient. (The anions of bacteriopheophytin and bacteriochlorophyll have very broad absorption extending throughout the 620−700 nm region, as is seen, for example, in the $P^+H_A^-$ spectrum of wild-type RCs in Figures 3B and 6.) Time constants for $P^+\beta^-$ charge recombination of ∼500 ps to 1 ns have been determined in a number of β-containing mutant RCs of both *Rb. capsulatus* and *Rb. sphaeroides* (*23*, *35*−*37*). It is not known what effect the Tyr → Phe mutation at M208 might have on the inherent lifetime of $P^+\beta^-$, except as might be indicated in this study. A time constant for $P^+H_B^- \rightarrow$ ground state charge recombination in the range of 1−4 ns has been estimated previously in the DH, KDH, and YFH mutant RCs in LDAO (*23*−*27*).

Against this background, we start with the simpler of the two cases, the YFHV+tb data, and continue to focus first on the 635−650 nm kinetic profiles. YFHV+tb is the simpler case because, with neither Q_A nor Q_B present, the decay on the nanosecond or tens of nanoseconds time scale reflects a combination of the $P^+\beta^- \rightarrow$ ground state and $P^+H_B^- \rightarrow$ ground state processes. Thus, the end point of the decay kinetics on the (tens of) nanosecond time scale for the YFHV+tb data (Figure 5) *must* be $\Delta A = 0$ at all probe wavelengths. This $\Delta A = 0$ constraint on the analysis of the YFHV+tb data means that the results are far less compromised by the fact that the longest time point is 3.7 ns (compared to the YFHV data analysis). Fitting of the 635−650 nm data for YFHV+tb to the sum of three exponentials plus a constant (fixed at 0) yields time constants of ∼30 ps, ∼200−300 ps, and ∼4−6 ns, where the ranges of values for the two longer time constants reflect acceptable fits that differ in the pre-exponential factors of these components. The 30 ps component is obvious in the raw data in Figure 5 as the initial fast phase of increasing absorption, corresponding to the transformation of the P* spectrum (0.5 ps spectrum) in Figure 3B to the one seen at 100 ps. The presence of a 200−300 ps component to decay of the 635−650 nm transient absorption is unambiguous from the fits (and even by visual inspection of the data), but not readily reconciled with the expected $P^+\beta^-$ and $P^+H_B^-$ charge recombination times discussed above. This component is in fact not associated with either of these two states, but rather with P* decay (*59*). Surprisingly, the decay of stimulated emission from P (monitored between 920 and 980 nm) is unambiguously biexponential, comprised of two components nearly equal in magnitude of ∼30 ps (55−60%) and ∼200 ps (40−45%). The 200 ps P* decay component also is observed in the decay of P bleaching (840−890 nm), thus reflecting a P* → ground state deactivation pathway that occurs in ∼45% of the sample (which may involve relaxation within P* or repopulation of P* from another transient state). Since P* obviously absorbs at 635−650 nm (0.5 ps spectra in Figure 3), both P* components must and do contribute to the anion region kinetic data. Since the 200−300 ps component is associated with P* → ground state deactivation, it contributes significantly to the *decay* portion of the kinetic profile at 635−650 nm.

Further description of P* decay will be given elsewhere (*59*). We have presented some details here to underscore the fact that the anion region kinetic data are part of a larger self-consistent body of data, and to show that the expected ∼200 ps P* kinetic component (along with the 30 ps component) is obtained de novo from analysis of the data in this region.[2] Recognition that P* decay is biexponential and both phases contribute in the anion region does not impair our analysis in determining the lifetimes of $P^+H_B^-$ in the presence and absence of Q_B (and thus, directly, the targeted rate constants k_{ET} and k_{CR}); the only difference is that a fourth exponential must be added to the fitting function describing the kinetic model.

Fitting the kinetic profiles to a function with eight free parameters—four exponentials (time constants) each with an

[2] Because a significant fraction of RCs (40-45%) returns to the ground state in ∼200 ps via the "delayed" P* decay component, the ultimate yield of electron transfer to the A side in YFHV+tb RCs isolated using Deriphat is smaller (25−30%) than that found previously (*12*) for YFH RCs isolated with LDAO (∼60%). The same is true for the YFHV and YFH samples studied here, so this phenomenon is not associated with either the W(M250)V mutation or the presence of terbutryn but appears to result from an effect of the detergent Deriphat, likely on the relative free energies of the states (*59*).

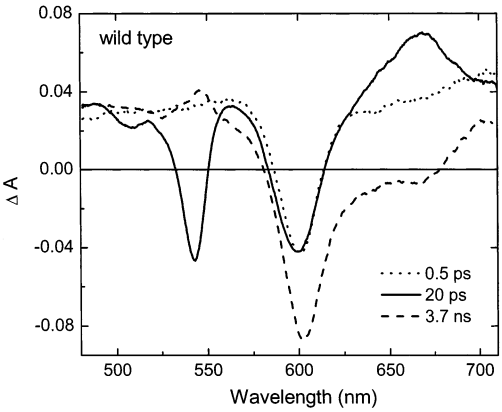

FIGURE 6: Transient absorption difference spectra for the wild type acquired at the indicated times following excitation with ~130 fs flashes at 860 nm.

associated amplitude (pre-exponential factors)—along with the long time constant asymptote still fixed to be $\Delta A = 0$, returns again the ~30 and ~200 ps components (assigned to P*) and, now, a time constant for each of the two longer components (due to $P^+H_B^-$ and $P^+\beta^-$). To determine the best value or range of values for the $P^+H_B^-$ charge recombination time that can be determined from the YFHV+tb data, we proceeded to apply two additional constraints on the analysis. (1) The time constants of the two initial components were fixed at 30 and 200 ps since these values are independently verified in the P*-stimulated emission data as described above (*59*), and (2) the third time constant was fixed at various values between 500 ps and 1 ns, in keeping with the reported range for the inherent $P^+\beta^-$ lifetime (*23*, *35*−*37*). In assessing the viability of individual fits, we considered not only how well the data were reproduced but also the values of the returned pre-exponential factors. These values directly reflect the relative concentrations and extinction coefficients of the species involved (P*, $P^+H_B^-$, and $P^+\beta^-$), about which we have much independent information from data obtained in this work and previous studies of RCs in which these same states are produced (*12*, *22*−*24*, *35*−*37*). Although we weight the values reported below using the fits with maximum constraints, considerable effort went into exploring the matrix of parameters (e.g., how many and which values were fixed) that can give good four-exponential fits of the data. One such fit of the YFHV+tb kinetic data is shown in Figure 5A (solid line). Our analysis suggests that the $P^+H_B^-$ lifetime τ_{TB} falls in the range of 4−8 ns; this result directly gives a rate constant k_{CR} of ~$(4-8\ \text{ns})^{-1}$ for the $P^+H_B^- \rightarrow$ ground state charge recombination process.

All of the above discussion for analyzing the anion region data for the YFHV+tb sample wholly pertains to analysis of the YFHV kinetic data, but with the additional complication that we do not know what ΔA is at the end point of the nanosecond-time scale decay (it can no longer be set at $\Delta A = 0$ because the long-lived $P^+Q_B^-$ is formed). However, we do have information that constrains the ΔA end point for the YFHV sample, as follows. Since $P^+\beta^- \rightarrow$ ground state is the only process that can occur on the A side in the YFHV sample (i.e., the end point of this decay process is $\Delta A = 0$ just as it is in the YFHV+tb data), any and all non-zero transient absorption changes at a sufficiently long time (tens of nanoseconds) necessarily directly reflect the yield of $P^+Q_B^-$ formation. Figure 6 shows the $P^+Q_A^-$ spectrum (3.7 ns) that is obtained for the 100% yield of this state in wild-type RCs (again normalized on the basis of the initial P* spectra in Figure 3). The value of ΔA in the range of 635−650 nm in this spectrum is −0.014. We assume that the $P^+Q_B^-$ spectrum in this region would be identical to the $P^+Q_A^-$ spectrum for the wild type. Thus, if $P^+H_B^- \rightarrow P^+Q_B^-$ electron transfer occurred with a 100% yield in the YFHV mutant, the observed ~30% yield of $P^+H_B^-$ would result in an ~30% yield of $P^+Q_B^-$. The value of ΔA at long times would be, then, $0.3(-0.014) = -0.004$. Thus, while the constant in the equation cannot be set equal to 0 (as in the YFHV+tb analysis), it is not a completely free parameter. It was constrained to be in the range of 0 to −0.004 based on this comparison to the wild-type spectrum.

A second critical consideration that constrains the analysis of YFHV anion region kinetic profiles is that the *only* other parameter (besides the value of the constant asymptote constrained above) that can be different between the YFHV+tb and YFHV data sets is the value of the longest kinetic component, i.e., the $P^+H_B^-$ lifetime. Therefore, the 30 and 200 ps P* components, the $P^+\beta^-$ component (varied between 0.5 and 1 ns), the values of pre-exponential factors of these three components, and the value of the pre-exponential factor of the $P^+H_B^-$ component were all the kept the same in pairs of fits that distinguished the $P^+H_B^-$ lifetimes (the longest component) in the YFHV versus the YFHV+tb data sets. This comparative analysis of the YFHV and YFHV+tb kinetic profiles in parallel yielded in all cases a shorter $P^+H_B^-$ lifetime for the YFHV data compared to the YFHV+tb data, as expected. An example fit of the YFHV data is shown in Figure 5A (- - -). This analysis gives a $P^+H_B^-$ lifetime τ_{QB} of ~1.5−3 ns in YFHV RCs, compared to a τ_{TB} of ~4−8 ns in the YFHV+tb sample.

A similar analysis of the time profiles for the appearance and decay of bleaching of the 527 nm Q_X band of H_B (Figure 5B) was conducted. The data plotted in Figure 5B are not the raw ΔA values between 522 and 533 nm, but rather the difference between the absorption changes in the 522−533 nm interval and those in the 570−585 nm interval; i.e., the plotted data are values of $\Delta A_{522-533} - \Delta A_{570-585}$. A "reference" region (570−585) is required because the *change* in ΔA at 522−533 nm as a function of time between 100 ps and 3.7 ns is extremely small; there is very little difference between the 100 ps and 3.7 ns spectra in Figure 4. The raw 522−533 nm absorption changes on the nanosecond time scale are much too small to attempt to fit. However, referenced against the positive background absorption of first P* and later P^+, the absorption changes reflecting the growth and subsequent decay of bleaching of the Q_X band of H_B can be followed. This is not to say that the data plotted for $\Delta A_{522-533} - \Delta A_{570-585}$ reflect the kinetics associated solely with the H_B pigment. Although the subtraction does lend a heavier weight to the relative contribution of the H_B pigment compared to the contributions of P* and P^+, the data must still be analyzed with four exponentials plus a constant. Much of the same discussion given above for the anion region, taking into account reasonable values for the asymptote of the decay at tens of nanoseconds and the relative extinction coefficients of the species being probed (P* absorption, P^+ absorption, and H_B bleaching), applies here as well, although there are differences in detail. As in the anion region, the initial 30 ps component associated with

Table 1: Estimates of the Rate and Yield of $P^+H_B^- \rightarrow P^+Q_B^-$ Electron Transfer

τ_{QB} (ns)[a]	τ_{TB} (ns)[a]	k_{ET}^{-1} (ns)[b]	Φ_{ET}[c]
1.5	4.0	2.4	0.62
1.5	8.0	1.9	0.81
3.0	4.0	12.0	0.25
3.0	8.0	4.8	0.62

[a] Values for the lifetimes of $P^+H_B^-$ as determined from four-exponential fits of the 635−650 nm kinetic data of YFHV (τ_{QB}) and YFHV+tb (τ_{TB}). [b] Calculated time constant for $P^+H_B^- \rightarrow P^+Q_B^-$ electron transfer determined from the values of τ_{QB} and τ_{TB}. With reference to Scheme 1, $\tau_{TB} = 1/k_{CR}$ and $\tau_{QB} = 1/(k_{CR} + k_{ET})$. [c] Calculated yield of the $P^+H_B^- \rightarrow P^+Q_B^-$ electron transfer reaction, where $\Phi_{ET} = k_{ET}/(k_{ET} + k_{CR})$.

P* decay is unambiguous in the data, here as the initial development of bleaching of the Q_X band of H_B. Again, in assessing the $P^+H_B^-$ lifetimes, we compared pairs of fits to the YFHV+tb and YFHV data that used identical values for all the parameters other than for the constant (asymptote) and the longest component (the $P^+H_B^-$ lifetime). The ranges of values for the $P^+H_B^-$ lifetimes that come from this analysis are as follows: $\tau_{TB} \sim 3-6$ ns and $\tau_{QB} \sim 1.5-2.5$ ns. Both of these ranges reflect lifetimes somewhat shorter than those that were obtained from analysis of the 635−650 nm data, although the agreement is quite good considering the difficulty of the task at hand. In particular, in both the anion and Q_X regions, the fits reproduce the conclusions drawn directly from the data in Figure 5 that the $P^+H_B^-$ lifetime in YFHV RCs is shorter when the Q_B site is fully occupied than when electron transfer to Q_B is inhibited. Because the analysis of the anion region data is more straightforward, we adopt the ranges of values obtained from the 635−650 nm kinetic profiles for subsequent calculations.

With a τ_{QB} of ∼1.5−3 ns and a τ_{TB} of ∼4−8 ns in hand, we can directly calculate k_{ET}, the rate of $P^+H_B^- \rightarrow P^+Q_B^-$ electron transfer, and the yield Φ_{ET} of this reaction, using the simple formulas given earlier. Comparison of the full range of values for the lifetimes gives a k_{ET} of $\sim(2-12\text{ ns})^{-1}$ and a Φ_{ET} of ∼25−80% for electron transfer from H_B^- to Q_B (Table 1, columns 3 and 4). Given that the absolute yield of $P^+H_B^-$ is 30−35%, this analysis predicts that overall $P^* \rightarrow P^+Q_B^-$ conversion occurs with a yield of ∼10−25%. More restrictive use of middle values of τ_{TB} and τ_{QB} gives a k_{ET} of $\sim(3-5\text{ ns})^{-1}$ and a Φ_{ET} of ∼60% for the rate and yield of $P^+H_B^- \rightarrow P^+Q_B^-$ electron transfer, respectively, which may be the most realistic to use in general discussions until accurate values are obtained from future experiments.

Concluding Remarks. We have resolved the first evidence of $P^+H_B^- \rightarrow P^+Q_B^-$ electron transfer as deduced from the absorbance changes associated with decay of $P^+H_B^-$ when electron transfer to Q_B is operative or inhibited. We have also shown that $P^+H_B^- \rightarrow P^+Q_B^-$ electron transfer occurs on the nanosecond time scale. Determination of the lifetime of $P^+H_B^-$ in the presence and the absence of Q_B straightforwardly gives the rate and yield of $P^+H_B^- \rightarrow P^+Q_B^-$ electron transfer. In practice, analysis of the kinetic profiles has limitations derived from the contributions of multiple species and processes at every wavelength, and a limited time span of the present measurements. Taking these issues into account, we estimate that $P^+H_B^- \rightarrow P^+Q_B^-$ electron transfer has a rate constant in the range of $(2-12\text{ ns})^{-1}$ and a yield in the range of 25−80%.

These results leave no doubt that $P^+H_B^- \rightarrow P^+Q_B^-$ electron transfer is at least 1 order of magnitude slower than $P^+H_A^- \rightarrow P^+Q_A^-$ electron transfer, which has a rate constant of $\sim(200\text{ ps})^{-1}$ and a yield of ∼100% in wild-type RCs. This is not a surprising result. Indeed, some may consider the fact that $P^+H_B^- \rightarrow P^+Q_B^-$ electron transfer takes place at all or that it occurs as fast as on the nanosecond time scale a somewhat surprising result. Q_B is functionally different from Q_A, and their respective binding pockets have many different characteristics (see refs *57* and *58* for reviews). Whereas Q_A is tightly bound in a closed and mostly hydrophobic environment, Q_B is loosely bound in a region that contains numerous ionizable amino acids. The function of Q_B is to receive two electrons from Q_A^- in successive turnovers of the RC photochemistry, and dissociate from the RC as the quinol (Q_BH_2). Thus, electron transfer and proton transfer to Q_B are intimately related. Q_A is strictly a one-electron acceptor and is never protonated. Influencing the electronic contribution to the rate of $P^+H_B^- \rightarrow P^+Q_B^-$ electron transfer is the issue of the equilibrium between the proximal and distal positions for Q_B (*62*−*65*). The location of Q_B in its binding site obviously dictates the distance between Q_B and H_B; again there is no parallel to the A side since Q_A is bound in a single position. A Trp residue at M250 situated between H_A and Q_A may act as a superexchange mediator to improve the electronic matrix element for $P^+H_A^- \rightarrow P^+Q_A^-$ electron transfer (*52*−*55*, *66*). The symmetry-related residue on the B side is a Phe at L216, which cannot serve this function to the same extent, possibly providing one contribution to slower $H^- \rightarrow Q$ electron transfer on the B branch.

The free energy changes (ΔGs) for the $P^+H_B^- \rightarrow P^+Q_B^-$ and $P^+H_A^- \rightarrow P^+Q_A^-$ reactions are similar but not identical. The B-side reaction may well have a somewhat larger free energy change, first because $P^+H_B^-$ is thought to be 100−150 meV higher in free energy than $P^+H_A^-$, due in part to differences in hydrogen bonding interactions (*6*, *7*, *12*, *13*, *23*, *67*−*69*). A second contribution to a larger ΔG is obtained if $P^+Q_B^-$ is lower in free energy than $P^+Q_A^-$.[3] It is possible that the reorganization energy for $P^+H_B^- \rightarrow P^+Q_B^-$ electron

[3] It is well-known that the ΔG for $P^+Q_A^- \rightarrow P^+Q_B^-$ electron transfer is −60 meV, the latter state being lower in energy (*75*). If it is assumed that the same $P^+Q_B^-$ state is formed from $P^+H_B^- \rightarrow P^+Q_B^-$ electron transfer, this would increase by 60 meV the ΔG for $P^+H_B^- \rightarrow P^+Q_B^-$ electron transfer compared to that for $P^+H_A^- \rightarrow P^+Q_A^-$ electron transfer. However, we have reported (*56*) in YFH RCs, where electron transfer occurs to Q_B via both the A and B branches, that in fact two distinct $P^+Q_B^-$ states are formed as evidenced by distinct biexponential kinetics of the decay of P bleaching. In YFH RCs, charge recombination of $P^+Q_B^-$ as formed from the A side occurs with a time constant of ∼1.5 s, whereas charge recombination of $P^+Q_B^-$ formed from the B side occurs with a time constant of >6 s. A number of previous studies have found very long lifetimes for $P^+Q_B^-$ charge recombination via the so-called direct route (*76*−*80*). A common interpretation of these results is that the free energy gap between $P^+Q_A^-$ and $P^+Q_B^-$ is larger than 60 meV. If this interpretation applies to YFH RCs, then $P^+Q_B^-$ as formed in YFH RCs via the B side is more than 60 meV below $P^+Q_A^-$. In turn, this would apply to the YFHV mutant as well, thereby contributing >60 meV to ΔG for $P^+H_B^- \rightarrow P^+Q_B^-$ electron transfer compared to $P^+H_A^- \rightarrow P^+Q_A^-$ electron transfer, in addition to the 100−150 meV contribution due to the free energy differences of $P^+H_A^-$ and $P^+H_B^-$ mentioned in the text. This discussion of energetics must be tempered, of course, by other factors such as conformational changes and proton uptake, both of which have yet to be explored as they relate to $P^+H_B^- \rightarrow P^+Q_B^-$ electron transfer. See ref *56* for further discussion.

transfer matches fairly well a larger ΔG due to the many ionizable groups in the Q_B binding pocket. However, the precise position of the $P^+H_B^- \rightarrow P^+Q_B^-$ electron transfer reaction on the Marcus rate (k_{ET}) versus ΔG curve is beyond the scope of this article. The main point of this discussion is simply to point out the possibility for myriad differences in the electronic and Franck−Condon (energetic) factors between the $P^+H_A^- \rightarrow P^+Q_A^-$ and $P^+H_B^- \rightarrow P^+Q_B^-$ electron transfer reactions. There is no a priori reason for $P^+H_B^- \rightarrow P^+Q_B^-$ to be optimized (with either a fast rate or a high yield) since this electron transfer reaction does not take place in vivo. In fact, there might be every reason to inhibit this process in an effort to optimize the two-electron gate function of Q_B. In this regard, it is interesting to note that not only is $P^+H_B^- \rightarrow P^+Q_B^-$ electron transfer a factor of ≥10 slower than the analogous process on the A branch, the inherent $P^+H_B^- \rightarrow$ ground state back reaction also appears to be significantly faster [$k_{CR} \sim (4-8\ ns)^{-1}$] than for the A-branch process $P^+H_A^- \rightarrow$ ground state [$\sim(20\ ns)^{-1}$]. Some origins for this difference between the back reaction rates have been discussed elsewhere (*23*) and will not be repeated here, except to note that the P^+H^- charge recombination rates are governed by electronic and energetic factors analogous to those mentioned above for the $P^+H^- \rightarrow P^+Q^-$ forward reactions and additionally include mixing with the higher-energy P^+B^- and P* states. The end result is that the rates of the electron transfer and charge recombination pathways of the P^+H^- states are clearly balanced to afford a higher yield of P^+Q^- on the A branch than on the normally inactive B pathway. Soon, we hope to further these comparisons by extending the time scale of our measurements to pinpoint the rate constants for the $P^+H_B^- \rightarrow P^+Q_B^-$ electron transfer and $P^+H_B^- \rightarrow$ ground state processes.

In addition to the insights described above, the results reported here should open up new avenues for exploring important issues associated with electron transfer to Q_B. Comparisons of the results of experiments that probe Q_B reduction via the B branch versus the normal Q_A pathway should prove to be valuable. There may also be interesting comparisons to plant systems. Photosystems I and II both have symmetric branches of potential electron carriers leading from a dimeric primary electron donor to a terminal acceptor, analogous to the bacterial RC. Currently, there is controversy with respect to whether electron transfer functionally takes place simultaneously through both branches of the PSI protein with overall electron transfer on one branch occurring much faster than on the other (*70*−*74*). The parallel to the work presented here is clear. Continued studies that further explore full dimer to quinone charge separation on the B branch not only will provide fundamental comparisons with the A-side processes in the bacterial RC but also may be of general value for helping to assess analogous issues in the plant photosystems.

REFERENCES

1. Deisenhofer, J., Epp, O., Miki, K., Huber, R., and Michel, H. (1985) *Nature 318*, 618−624.
2. Yeates, T. O., Komiya, H., Chirino, A., Rees, D. C., Allen, J. P., and Feher, G. (1988) *Proc. Natl. Acad. Sci. U.S.A. 85*, 7993−7997.
3. El-Kabbani, O., Chang, C. H., Tiede, D. M., Norris, J. R., and Schiffer, M. (1991) *Biochemistry 30*, 5361−5369.
4. Ermler, U., Fritsch, G., Buchanan, S. K., and Michel, H. (1994) *Structure 2*, 925−936.
5. Deisenhofer, J., Epp, O., Sinning, I., and Michel, H. (1995) *J. Mol. Biol. 246*, 429−457.
6. Parson, W. W., Chu, Z. T., and Warshel, A. (1990) *Biochim. Biophys. Acta 1017*, 251−272.
7. Gunner, M. R., Nicholls, A., and Honig, B. (1996) *J. Phys. Chem. 100*, 4277−4291.
8. Bixon, M., Jortner, J., and Michel-Beyerle, M. E. (1995) *Chem. Phys. 197*, 389−404.
9. Schmidt, S., Arlt, T., Hamm, P., Huber, H., Nagele, T., Wachtveitl, J., Meyer, H., Scheer, H., and Zinth, W. (1994) *Chem. Phys. Lett. 223*, 116−120.
10. Steffen, M. A., Lao, K., and Boxer, S. G. (1994) *Science 264*, 810−816.
11. Pudlak, M., and Pincak, R. (2001) *Chem. Phys. Lett. 342*, 587−592.
12. Kirmaier, C., He, C., and Holten, D. (2001) *Biochemistry 40*, 12132−12139.
13. Katilius, E., Katiliene, Z., Lin, S., Taguchi, A. K. W., and Woodbury, N. W. (2002) *J. Phys. Chem. B 106*, 1471−1475.
14. Bixon, M., Jortner, J., Michel-Beyerle, M. E., and Ogrodnik, A. (1989) *Biochim. Biophys. Acta 977*, 273−286.
15. Scherer, P. O. J., and Fischer, S. F. (1989) *Chem. Phys. 131*, 115−127.
16. Zhang, L. Y., and Friesner, R. A. (1998) *Proc. Natl. Acad. Sci. U.S.A. 95*, 13603−13605.
17. Michel-Beyerle, M. E., Plato, M., Deisenhofer, J., Michel, H., Bixon, M., and Jortner, J. (1988) *Biochim. Biophys. Acta 932*, 52−70.
18. Ivashin, N., Kallebring, B., Larsson, S., and Hansson, O. (1998) *J. Phys. Chem. B 102*, 5017−5022.
19. Hasegawa, J., and Nakatsuji, H. (1998) *J. Phys. Chem. B 102*, 10420−10430.
20. Kolbasov, D., and Scherz, A. (2000) *J. Phys. Chem. B 104*, 1802−1809.
21. King, B. A., deWinter, A., McAnaney, T. B., and Boxer, S. G. (2001) *J. Phys. Chem. B 105*, 1856−1862.
22. Heller, B. A., Holten, D., and Kirmaier, C. (1995) *Science 269*, 940−945.
23. Kirmaier, C., Weems, D., and Holten, D. (1999) *Biochemistry 38*, 11516−11530.
24. Roberts, J. A., Holten, D., and Kirmaier, C. (2001) *J. Phys. Chem. B 105*, 5575−5584.
25. Czarnecki, K., Kirmaier, C., Holten, D., and Bocian, D. F. (1999) *J. Phys. Chem. A 103*, 2235−2246.
26. Kirmaier, C., Laible, P. D., Czarnecki, K., Hata, A. N., Hanson, D. K., Bocian, D. F., and Holten, D. (2002) *J. Phys. Chem. B 106*, 1799−1808.
27. Kirmaier, C., Cua, A., He, C., Holten, D., and Bocian, D. F. (2002) *J. Phys. Chem. B 106*, 495−503.
28. Katilius, E., Turanchik, T., Lin, S., Taguchi, A. K. W., and Woodbury, N. W. (1999) *J. Phys. Chem. B 103*, 7386−7389.
29. Lin, S., Jackson, J. A., Taguchi, A. K. W., and Woodbury, N. W. (1999) *J. Phys. Chem. B 103*, 4757−4763.
30. Lin, S., Katilius, E., Haffa, A. L., Taguchi, A. K., and Woodbury, N. W. (2001) *Biochemistry 40*, 13767−13773.
31. Kellogg, E. C., Kolaczkowski, S., Wasielewski, M. R., and Tiede, D. M. (1989) *Photosynth. Res. 22*, 47−59.
32. Gray, K. A., Wachtveitl, J., and Oesterhelt, D. (1992) *Eur. J. Biochem. 207*, 723−731.
33. de Boer, A. L., Neerken, S., de Wijn, R., Permentier, H. P., Gast, P., Vijgenboom, E., and Hoff, A. J. (2002) *Biochemistry 41*, 3081−3088.
34. de Boer, A. L., Neerken, S., de Wijn, R., Permentier, H. P., Gast, P., Vijgenboom, E., and Hoff, A. J. (2002) *Photosynth. Res. 71*, 221−239.
35. Kirmaier, C., Gaul, D., DeBey, R., Holten, D., and Schenck, C. C. (1991) *Science 251*, 922−927.
36. Kirmaier, C., Laporte, L., Schenck, C. C., and Holten, D. (1995) *J. Phys. Chem. 99*, 8910−8917.
37. Heller, B. A., Holten, D., and Kirmaier, C. (1996) *Biochemistry 35*, 15418−15427.
38. Nagarajan, V., Parson, W. W., Gaul, D., and Schenck, C. (1990) *Proc. Natl. Acad. Sci. U.S.A. 87*, 7888−7892.
39. Nagarajan, V., Parson, W. W., Davis, D., and Schenck, C. C. (1993) *Biochemistry 32*, 12324−12336.

40. Chan, C.-K., Chen, L. X.-Q., DiMagno, T. J., Hanson, D. K., Nance, S. L., Schiffer, M., Norris, J. R., and Fleming, G. R. (1991) *Chem. Phys. Lett. 176*, 366−372.
41. Du., M., Rosenthal, S. J., Xie, X., DiMagno, T. J., Schmidt, M., Hanson, D. K., Schiffer, M., Norris, J. R., and Fleming, G. R. (1992) *Proc. Natl. Acad. Sci. U.S.A. 89*, 8517−8521.
42. Jia, Y., DiMagno, T. J., Chan, C.-K., Wang, Z., Du, M., Hanson, D. K., Schiffer, M., Norris, J. R., Fleming, G. R., and Popov, M. S. (1993) *J. Phys. Chem. 97*, 13180−13191.
43. Finkele, U., Lauterwasser, C., Zinth, W., Gray, K. A., and Oesterhelt, D. (1990) *Biochemistry 29*, 8517−8521.
44. Hamm, P., Gray, K. A., Oesterhelt, D., Feick, R., Scheer, H., and Zinth, W. (1993) *Biochim. Biophys. Acta 1142*, 99−105.
45. Alden, R. G., Parson, W. W., Chu, Z. T., and Warshel, A. (1996) *J. Phys. Chem. 100*, 16761−16770.
46. Beekman, L. M. P., van Stokkum, I. H. M., Monshouwer, R., Rijnders, A. J., McGlynn, P., Visschers, R. W., Jones, M. R., and von Grondelle, R. (1996) *J. Phys. Chem. 100*, 7256−7268.
47. Laible, P. D., Greenfield, S. R., Wasielewski, M. R., Hanson, D. K., and Pearlstein, R. M. (1997) *Biochemistry 36*, 8677−8685.
48. Streltsov, A. M., Vulto, S. I. E., Shkuropatov, A. Y., Hoff, A. J., Aartsma, T. J., and Shuvalov, V. A. (1998) *J. Phys. Chem. B 102*, 7293−7298.
49. Zhou, H., and Boxer, S. G. (1998) *J. Phys. Chem. B 102*, 9139−9147.
50. Jones, M. R., Heer-Dawson, M., Mattioli, T. A., Hunter, C. N., and Robert, B. (1994) *FEBS Lett. 339*, 18−24.
51. Laible, P. D., Kirmaier, C., Holten, D., Tiede, D. M., Schiffer, M., and Hanson, D. K. (1998) in *Photosynthesis: Mechanisms and Effects* (Garab, G., Ed.) pp 849−852, Kluwer Academic Publishers, Dordrecht, The Netherlands.
52. Coleman, W. J., Bylina, E. J., Aumeier, W., Siegl, J., Eberl, U., Heckmann, R., Ogrodnik, A., Michel-Beyerle, M. E., and Youvan, D. C. (1990) in *Structure and Function of Bacterial Photosynthetic Reaction Centers* (Michel-Beyerle, M. E., Ed.) pp 273−281, Springer-Verlag, New York.
53. Coleman, W. J., and Youvan, D. C. (1990) *Annu. Rev. Biophys. Biophys. Chem. 19*, 333−367.
54. Stilz, H. U., Finkele, U., Holzapfel, W., Lauterwasser, C., Zinth, W., and Oesterhelt, D. (1990) in *Structure and Function of Bacterial Photosynthetic Reaction Centers* (Michel-Beyerle, M. E., Ed.) pp 265−271, Springer-Verlag, New York.
55. Stilz, H. U., Finkele, U., Holzapfel, W., Lauterwasser, C., Zinth, W., and Oesterhelt, D. (1994) *Eur. J. Biochem. 223*, 233−242.
56. Laible, P. D., Kirmaier, C., Udawatte, C. S. M., Hoffman, S. J., Holten, D., and Hanson, D. K. (2003) *Biochemistry* (in press).
57. Sebban, P., Maroti, P., and Hanson, D. K. (1995) *Biochimie 77*, 677−694.
58. Okamura, M. Y., Paddock, M. L., Graige, M. S., and Feher, G. (2000) *Biochim. Biophys. Acta 1458*, 148−163.
59. Kirmaier, C., Laible, P. D., Hinden, E., Hanson, D. K., and Holten, D. (2003) *Chem. Phys.* (manuscript in preparation).
60. Kirmaier, C., and Holten, D. (1991) *Biochemistry 30*, 609−613.
61. Yang, S. I., Li, J., Cho, H. S., Kim, D., Bocian, D. F., Holten, D., and Lindsey, J. S. (2000) *J. Mater. Chem. 10*, 283−296.
62. Kleinfeld, D., Okamura, M. Y., and Feher, G. (1984) *Biochemistry 23*, 5780−5786.
63. Stowell, M. H., McPhillips, T. M., Rees, D. C., Soltis, S. M., Abresch, E., and Feher, G. (1997) *Science 276*, 812−816.
64. Pokkuluri, P. R., Laible, P. D., Deng, Y. L., Wong, T. N., Hanson, D. K., and Schiffer, M. (2002) *Biochemistry 41*, 5998−6007.
65. Xu, Q., Baciou, L., Sebban, P., and Gunner, M. R. (2002) *Biochemistry 41*, 10021−10025.
66. Plato, M., Michel-Beyerle, M. E., Bixon, M., and Jortner, J. (1989) *FEBS Lett. 249*, 70−74.
67. Thompson, M. A., and Zerner, M. (1991) *J. Am. Chem. Soc. 113*, 8210−8215.
68. Marchi, M., Gehlen, J. N., Chandler, D., and Newton, M. (1993) *J. Am. Chem. Soc. 115*, 4178−4190.
69. Blomberg, M. R. A., Siegbahn, P. E. M., and Babcock, G. T. (1998) *J. Am. Chem. Soc. 120*, 8812−8824.
70. Yang, F., Shen, G., Schluchter, W. M., Zybailov, B. L., Ganago, A. O., Vassiliev, I. R., Bryant, D. A., and Golbeck, J. H. (1998) *J. Phys. Chem. B 102*, 8288−8299.
71. Joliot, P., and Joliot, A. (1999) *Biochemistry 38*, 11130−11136.
72. Guergova-Kuras, M., Boudreaux, B., Joliot, A., Joliot, P., and Redding, K. (2001) *Proc. Natl. Acad. Sci. U.S.A. 98*, 4437−4442.
73. Muhiuddin, I. P., Heathcote, P., Carter, S., Purton, S., Rigby, S. E. J., and Evans, M. C. E. (2001) *FEBS Lett. 503*, 56−60.
74. Rigby, S. E. J., Muhiuddin, I. P., Evans, M. C. W., Purton, S., and Heathcote, P. (2002) *Biochim. Biophys. Acta 1556*, 13−20.
75. Kleinfeld, D., Okamura, M. Y., and Feher, G. (1984) *Biochim. Biophys. Acta 766*, 126−140.
76. Takahashi, E., and Wraight, C. A. (1992) *Biochemistry 31*, 855−866.
77. Labahn, A., Paddock, M. L., McPherson, P. H., Okamura, M. Y., and Feher, G. (1994) *J. Phys. Chem. 98*, 3417−3423.
78. Labahn, A., Bruce, J. M., Okamura, M. Y., and Feher, G. (1995) *Chem. Phys. 197*, 355−366.
79. Allen, J. P., Williams, J. C., Graige, M. S., Paddock, M. L., Labahn, A., Feher, G., and Okamura, M. Y. (1998) *Photosynth. Res. 55*, 227−233.
80. Schmid, R., and Labahn, A. (2000) *J. Phys. Chem. B 104*, 2928−2936.

BI026973O